Laboratory experiments in atmospheric optics

Michael Vollmer and Robert Tammer

Old and new laboratory experiments on atmospheric optics with a focus on mirages, rainbows, and halos are presented. Some qualitative demonstrations serve primarily didactical purposes, e.g., by proving the existence of curved light rays in media with a gradient of the index of refraction, by directly visualizing the minimum-deviation curve for rainbow paths in water droplets, or by helping to elucidate the ray classes in hexagons that contribute to a specific halo. In addition, quantitative experiments allow a direct comparison of angular positions and intensities with analytical computations or Monte Carlo simulations of light scattering from small water droplets or ice hexagons. In particular, the latter can help us to understand complex halo phenomena. © 1998 Optical Society of America

OCIS codes: 010.0010, 010.1290, 010.2940, 010.4030.

1. Introduction

If you love nature, you respond to her phenomena as naturally as you breathe . . . Never think that the poetry of nature's moods in all their infinite variety is lost on the scientific observer, for the habit of observing refines our sense of beauty and adds a brighter hue to the richly colored background against which each particular fact is outlined.

These words of Marcel Minnaert in the preface of his famous book, *Light and Color in the Outdoors*[1] from 1937, expressed his feelings when he was observing nature. They still describe the major motivation for current research of many people who nowadays scientifically investigate phenomena of the nature around us. In most fields of physics and other natural sciences, research is based on the interplay of theory and experiment that leads to a scientific understanding. Concerning atmospheric optics, the field of interest appears, however, not to be twofold but rather threefold (this division does not refer to individual researchers, who might belong to several of these groups).

First, there are the true observers of nature in the sense of Minnaert, who carry out naked-eye observations or use optical instruments like binoculars or telescopes. Usually the observations are documented in the form of slides or photographs; lately transient phenomena are often recorded by videocameras. These observations are the raw material of atmospheric optics research.

Second, the theoreticians use this raw material of observations and try to give qualitative as well as quantitative explanations. Depending on the phenomenon under study, quite elaborate theoretical approaches have to be applied, ranging, e.g., from classical electrodynamics for simple spherical geometry (Mie theory) to complex multiple-scattering Monte Carlo simulations for nonspherical geometries.

The third approach to atmospheric optics is based on the experimental point of view. Many optical phenomena of the atmosphere can be simulated in the laboratory. Hence optical phenomena of the atmosphere can also be quantitatively studied under well-defined conditions and for longer time periods than those available in nature. Experimental rainbows, halos, or mirages can therefore help us to understand the natural phenomena, to demonstrate them to interested people, and to perform quantitative tests of the theories (as a matter of fact, every theory, explaining a natural phenomenon, should also be tested quantitatively in a laboratory experiment concerning angular positions as well as intensities).

Below, a survey of simple and complicated, old and new, and qualitative as well as quantitative laboratory experiments of atmospheric optics is given. On the one hand, it should serve didactical purposes. Because atmospherical optical phenomena are particularly well suited to arouse scientific interest in school children of all ages, it seems helpful for teachers to have a selection of easy and impressive lecture

The authors are with the Physikalische Ingenieurwissenschaften, Fachhochschule Brandenburg, Magdeburgerstrasse 50, 14770 Brandenburg, Germany.

Received 25 June 1997; revised manuscript received 29 September 1997.

0003-6935/98/091557-12$15.00/0

Reprint from 20 March 1998 / Vol. 37, No. 9 / Applied Optics 1557 - 1568

Fig. 1. Mirage in the desert (from Ref. 6).

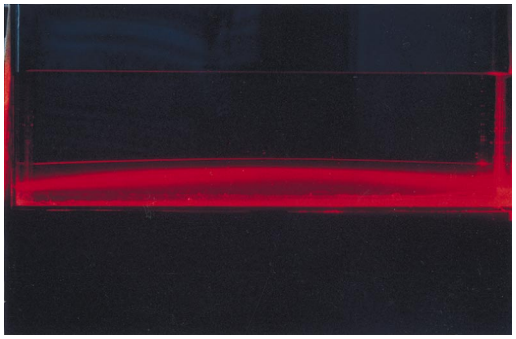

Fig. 2. Curved He–Ne laser beam in a tank with fresh water on top of saturated salt water, i.e., an artificial inversion layer.

demonstrations at various levels of difficulty at hand. In addition, specific sophisticated theoretical explanations of these phenomena can be directly visualized, e.g., the minimum-deviation curve for rainbow paths in water droplets or the ray classes in hexagons contributing to a specific halo.

On the other hand, quantitative laboratory experiments allow direct comparison with the partially complex up-to-date analytical computations or Monte Carlo simulations of light scattering from small water droplets or ice hexagons. In particular the latter can help us to understand complex halo phenomena.

The elementary theories of the various phenomena are not outlined here in detail, as many good treatments can be found in the literature (e.g., Refs. 1–4). Rather, short descriptions of the physical processes are given with emphasis on the experimental simulation, in particular of mirages, rainbows, and halos. The state of the art can be found in the special features on light and color in the open air.[5]

2. Mirage Experiments

An old artistic view of a mirage in a desert scene is shown in Fig. 1. In brief, mirage effects occur because of a curvature of light rays, bent in the air because of a gradient of the index of refraction, which is a consequence of different temperatures. Simple demonstration experiments of mirages are classified according to these various curved light paths; consequently the two major experimental setups refer to superior and inferior mirages. A prerequisite to both kinds of mirages is the demonstration of curved light rays in inhomogeneous media.

A recent excellent description of laboratory simulations of inferior and superior mirages was given by Greenler.[7] The basic setups used here are similar. New aspects concern the differences of the object distances of the real image compared with those of the mirage and the possibility of also observing transient effects of mirages due to turbulences of the medium (which in nature is air, in the experiment a liquid).

A. Curved Light Rays

The curvature of light paths can be demonstrated easily in liquids with a gradient of the index of refraction.[7–9] The equipment needed consists of only a water tank (dimensions, e.g., 10 cm × 30 cm × 20 cm height), a light beam (e.g., from a He–Ne laser), and layered sugar or salt solutions.

The solutions may be prepared in a variety of ways. Below the procedure for only the salt solution is described. Either fresh water is poured on top of a saturated salt solution or a saturated salt solution is poured below the fresh water layer by means of a regulated flow through a thin rubber tube, ending at the bottom of the tank. In both cases one can generate the layered systems without much mixing by carefully avoiding turbulences and vibrations on filling the tank.

After preparation, the two liquids slowly mix by diffusion processes, resulting in a gradient of the index of refraction between the saturated salt solution ($n \approx 1.364$) and pure water ($n \approx 1.332$) at $\lambda = 632.8$ nm (hence this setup corresponds qualitatively to an inversion layer in the atmosphere in which warm air is above colder air). The water tank should not be exposed to vibrations, as rapid diffusion decreases the period for observations. Without disturbing the solution, experiments for demonstration of curved light beams may be performed for a couple of hours, those of three-part superior mirages for even longer times, and some mirage distortions, like towering or stooping, may be seen for 1 or 2 days.

After preparation of the layered liquids in the tank, the curvature of a He–Ne laser in the inhomogeneous solution can be easily demonstrated by illumination from below and varying of the angle of incidence. Figure 2 is a photograph of a curved laser beam directed through the tank and viewed from the side.

Even a horizontally incident beam will be curved downward because of the vertical gradient of the index of refraction. This is due to the finite dimension at the beam waist: the upper and the lower portions will be bent differently and consequently the whole ray will be curved.

B. Inferior Mirage

Inferior mirages, i.e., desert mirages, have already been simulated nearly 100 years ago by Wood[10] and repeated by Greenler.[7] In nature, these mirages are observed over distances of hundreds of meters to kilometers. Nowadays the most usual observations are on the pavement of hot streets on summer days.

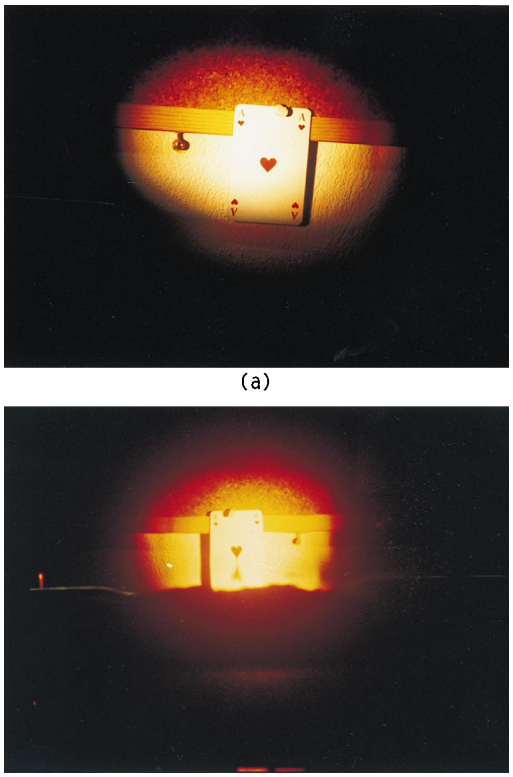

Fig. 3. Object, like the ace of hearts, (a) observed over a hot metal plate (length 3 m) gives rise to (b) an inferior mirage. Total distance from object to observer ≈6 m, focal length 210 mm.

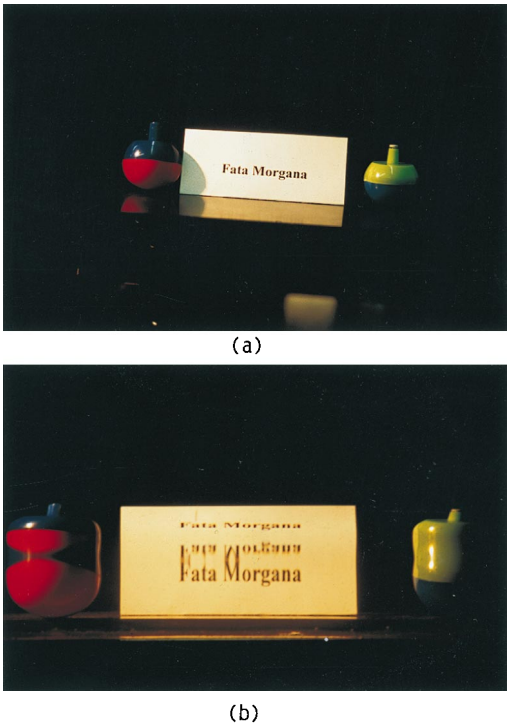

Fig. 4. Objects (two colored tops and the words FATA MORGANA) as viewed through (a) plain water, (b) the artificial inversion layer. The three-part mirage in (b) corresponds to a superior mirage.

Typical laboratory dimensions are smaller by a factor of ~1000; hence the temperature differences have to be higher or the objects smaller. Usually a plate of metal (several meters long) is heated (e.g., by gas flames, which by itself is a spectacular demonstration). Following Greenler, covering the plate with a layer of sand ensures that no actual reflections from the metal are possible. During the heating, a He–Ne laser beam directed parallel to the surface of the plate through the hot air fluctuates, a phenomenon well known to every astronomer. Figure 3 depicts a mirage seen above such a hot plate. In this case, the object was a playing card, the ace of hearts. Other examples of good quality were published by Greenler.[7]

C. Superior Mirage

Superior mirages may be observed with the water tank setup described above. Curved light paths, i.e., the prerequisites for mirages, were demonstrated in Fig. 2. Hence one may readily observe mirages of objects through the water tank. The sizes of the objects depend on the height of the salt solution and the fresh water layers. Typically we used dimensions of several centimeters. Parameters for the mirages are the orientation of the object with respect to the artificial inversion layer [i.e., the relative height of the object and the boundary (diffusion) layer and the distance of the object behind the water tank], the distance of the observer, and the angle of incidence of light rays with respect to the eye of the observer. Consequently the way of observing mirages and optimizing the conditions is to use a selected distance and height of the object with respect to the boundary layer and vary the observation angle and distance by moving the eye. Optimum conditions are usually found within a couple of minutes. In order to have better quality of the mirages, we illuminated the objects and—to reduce light attenuation while passing the liquids—we observed through the smaller dimension (width) of typically 10 cm rather than through the length of the tank. Depending on the observation angles, one can readily observe three-part images (see Fig. 4) or just stooping or towering. These effects correspond to the well-known mirages due to inversion layers in the atmosphere. In nature, the dimensions are of the order of kilometers and changes of the index of refraction are of the order of several 10^{-5}. The reason for easy observation in the laboratory is obvious: In the experiment, the artificial inversion layer has changes of the index of refraction of the order of 10^{-2} and dimensions are consequently reduced to ~1 m.

For large audiences it is convenient to use a videocamera on a tripod combined with a videoprojector. By adjusting the height of the camera and correspondingly changing the angle of observation, one can demonstrate the change of the mirages from the single image of the object (viewed through a single solution) stooping or towering and finally to three-part mirages.

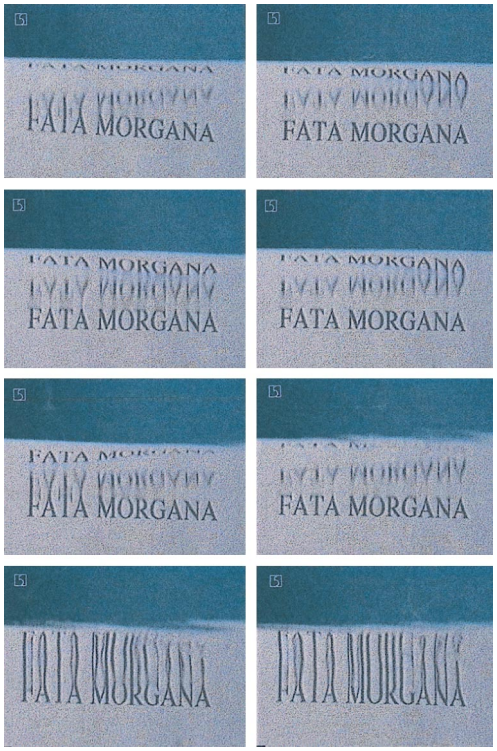

Fig. 5. Snapshots of a videosequence of transient effects in mirages due to wavelike disturbences. Some parts of the mirages vanish and reappear periodically.

Systematic investigations of these artificial mirages, in particular the use of videocameras to record the effects, reveal another interesting property. In order to focus the object and the mirages simultaneously, it is necessary to select a large *f*-number (small aperture), i.e., the light rays forming the image of the object and those of the mirages seem to come from different object distances. While observing with the naked eye, one automatically accommodates and hence observes all images as focused.

One of the most fascinating properties of mirages in nature is the transient effects that are due to air fluctuations. One can demonstrate this by introducing water turbulences, e.g., by slowly stirring the system. Wavelike disturbances in the artificial inversion layer lead to similar wavelike patterns in the mirages. This can be most easily demonstrated by video sequences. Figure 5 shows a number of snapshots from such a sequence, taken at time intervals of the order of seconds (see Ref. 11).

D. Other Recipes

Laboratory simulations of mirages can also be easily demonstrated with sugar solutions.[12] In particular, multilayer solutions that help us to understand more complex mirages in nature are possible. Quite a few more complicated chemical recipes have also been reported in the literature (e.g., Ref. 8). In most cases, however, controlled substances are required. Therefore they are not suited for simple lecture demonstrations.

3. Rainbow Experiments

In brief, the classical geometric optical explanation of the rainbow is based on the interaction of light with a single droplet. Parallel light is incident upon a raindrop. According to the laws of refraction and reflection, the angular deviation due to light rays producing the primary rainbow is calculated as a function of the impact parameter for given index of refraction. Because of a shallow minimum of this curve, the light intensity as a function of angle exhibits a sharp peak of deflected light intensity (Descartes was the first to estimate this minimum-deviation effect numerically). Similar arguments hold for higher-order rainbows.

Geometric optics does not properly describe the rainbow with all details. In particular the concept of interference leads to easily observable discrepancies between the predictions of the geometric theory and the observations of supernumerary arcs. The geometric optics intensity profile must be substituted by interference rings (Airy rings), with the position of the first maximum being shifted. Quantitative analysis uses either the approximate Airy theory or the complete Mie theory.[5,13–15]

Qualitative and quantitative experimental demonstrations are described below. For example, the minimum-deviation effect curve can be directly proved, and Airy ring systems can be measured for spherical and cylindrical symmetry. The first experiments of this kind had already been performed in the Middle Ages (see Ref. 16), but many refinements are due to later ages, including our century after the invention of the laser.

A. Setup for Rainbow Experiments

The general setup for a demonstration of rainbows consists of a light source, raindrops, and a detector or observation screen placed at an appropriate angle. Polarizing sheets are helpful. Because the main features of a rainbow can be understood with the minimum-deviation curve related to a single drop,[17,18] most experiments just study the behavior of a single drop. As white-light sources, one can use, e.g., simple halogen lamps or arc lamps with condensing optics (for qualitative purposes, slide projectors or overhead projectors are sufficient), He–Ne lasers are easily accessible monochromatic sources. The usual detector for rainbows is the human eye; however, quantitative experiments are possible with photodiodes or similar devices. As raindrops, one can, for example, use water drops from the needle of a syringe. However, experiments are also possible with other liquid materials or glass spheres, etc. Hence, in order to compare results for materials with different indices of refraction n, the rainbow angles (order N) must be computed from the geometric optics formula,

$$\cos^N(\alpha_{\mathrm{inc}}) = \left[\frac{n^2 - 1}{(N+1)^2 - 1}\right]^{1/2}. \qquad (1)$$

Here α_{inc} is the angle of incidence for the respective rainbow rays, which gives the deviation angle δ according to

$$\delta(\alpha_{inc}) = 2\alpha_{inc} + (N + 1)(\pi - 2\alpha_{refr}) - \pi, \qquad (2)$$

where the angle of the refracted ray α_{refr} is computed from Snell's law.

B. White-Light Rainbows: Direct Demonstration of Minimum-Deviation Curve

The minimum deviation curve can be directly tested. For this purpose, it is useful to have a large drop and small light beam diameters. In our setup, we used a 6.5-cm glass sphere and white light from an arc lamp with a diameter of 0.5 cm. First the sphere is adjusted on axis with the light beam. This results in two overlapping white spots of reflected light on the axis. Subsequently the light beam is moved sideways relative to the sphere (in principle, either of the two can be moved). Consequently the two white-light spots in the backward direction are now separated on the screen. The first one is due to reflection at the surface of the sphere, the second one to light rays of the rainbow type, i.e., first refraction into the sphere, one internal reflection, and second refraction while exiting the sphere. For small impact parameters ($b/R \leq 0.7$) both spots remain white. Increasing the impact parameter leads to a blurring out of the rainbow spot. Approaching the rainbow value of $b/R = 0.86$ suddenly leads to a colorful spot at the rainbow angle. Increasing the angle further leads to a change of direction of this spot while it is blurring out while also turning white again. As $b = R$ is approached, it can be clearly seen that the deviation angle is finite and smaller than 180°. In a darkened room, one may also observe a third more faint white spot that moves opposite to the one of the primary rainbow rays. For b/R slightly larger than the one of the primary bows, this spot develops the secondary rainbow. For quantitative measurement of the even smaller differences in b/R for the minima for higher-order rainbows, the use of a precise translational stage is recommended.

Illumination of single drops by white light, e.g., from an arc lamp, leads to fascinating caustic effects due to gravitational and adhesion effects suffered by the drop. Figure 6 depicts the white-light rainbow (or rather the caustic patterns) of a single water drop of ~1-mm size.

In principle, the minimum-deviation effect can also be demonstrated with a laser; however, in this case, no colorful bands, but rather the occurrence of the Airy ring systems (see below) is the criterion for the proper impact parameter.

A big water droplet can also be simulated by a glass sphere filled with water or for less didactical purposes with wine or similar liquids (which need not be put into the drain at the end of the show). In addition to changes of the angle itself (method for determining the index of refraction), the relative intensities change according to Fresnel's equations.

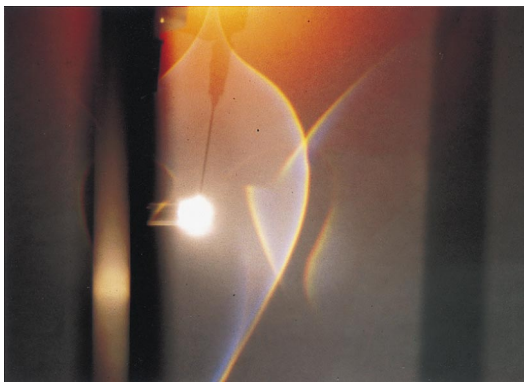

Fig. 6. Rainbow caustics of a single water droplet, illuminated by white light from an arc lamp.

The predominantly perpendicular polarization of rainbows[19] can be easily tested with polarizing filters. Placing, e.g., a polarizing foil between the drop and the screen shows noticeable intensity differences. Of course the perpendicular polarization relates to the plane of incidence, which itself depends on the position in the bow. Consequently the polarization of the light on top of the bow is rotated by 90° compared with the light at the sides.

C. Rainbow Light Paths of Primary and Higher-Order Rainbows

For small beam diameters compared with the sphere diameter, it is also possible to visualize directly the ray paths that are responsible for the primary, secondary, and higher-order rainbows. For the glass sphere, the observability depends on the quality of the glass, as the light beam is visible only when scattered at impurities or fluctuations of the index of refraction. It is easier to use water, e.g., in a glass cup with thin sides. Fresh tap water works best because it has many impurities whereas distilled water shows much less scattering. Figure 7 shows the light paths of a 5-mW He–Ne laser in a glass filled with water for impact parameters $b/R > 0.86$, i.e., in the region of the higher-order rainbow rays as well as the theoretical ray paths according to Ref. 20.

Because the rainbow ray impact parameters correspond to angles of incidence near the critical angle, internal reflections are quite efficient and many higher-order ray paths can be seen. Following the incident light ray allows us to correlate the exiting rays to a specific ray class that is responsible for the higher-order bows. Because of the finite width of the glass the shown example is qualitative only, i.e., the rainbow angles are not quantitatively in accordance with those of pure water. For optimal observation the glass should have a nearly cylindrical shape at the position of the light beam.

D. Qualitative Demonstration of Airy Rings with Monochromatic Light

Direct observation of interference effects in rainbows is most easily possible with a He–Ne laser and a water drop. As a matter of fact, this is the most

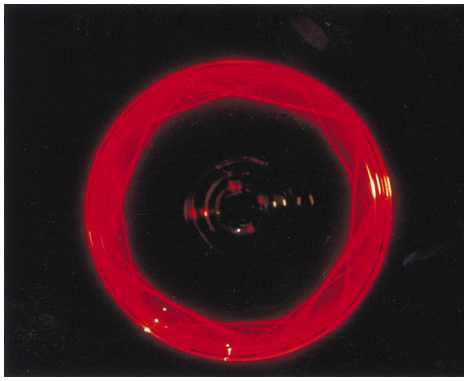

(a)

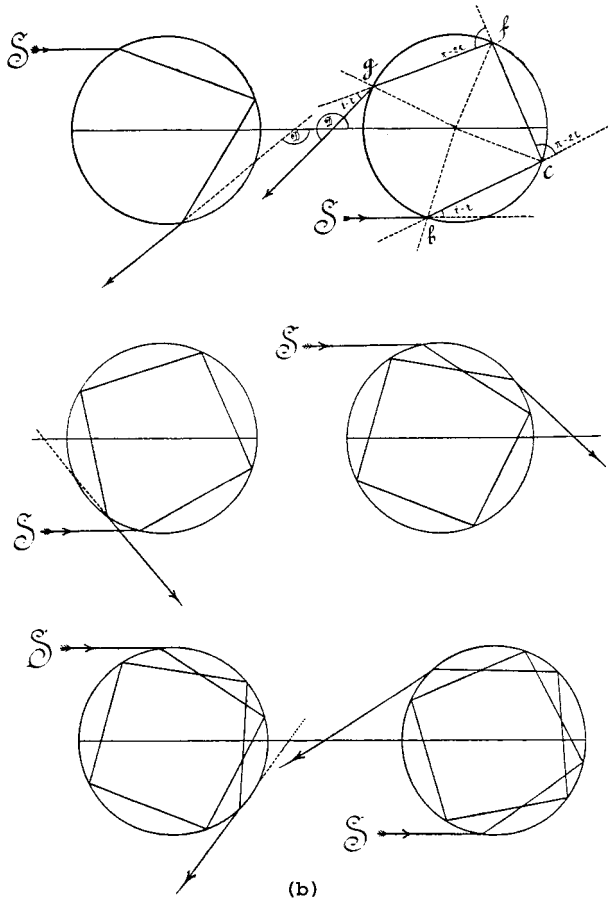

(b)

Fig. 7. Experimentally observed rainbow light paths of higher-order rainbows within (a) the water drop, (b) the theoretical ray paths (after Ref. 20).

simple imaginable interference experiment with a laser, as one needs only a single drop of water to observe spectacular displays.

Credit for this kind of experiment goes to Walker, who performed a series of easy and instructive experiments[21] (see also Ref. 22). He reported observation of higher-order bows up to the 13th order by successively blocking smaller impact parameter regions that give rise to smaller-order rainbows. This blocking of inner impact parameter regions is not trivial. For example, the minimum-deviation impact parameter for the sixth-order rainbow has already reached the value $b/R = 0.99$ for $n = 1.330$. In this respect, careful observations are more tedious than expected after one has read these excellent articles.

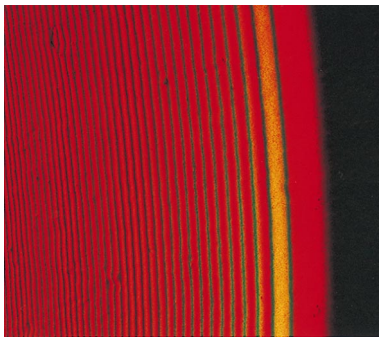

Fig. 8. Airy ring systems of primary bow due to illumination with two colinear red and green He–Ne lasers.

Direct observation of Airy ring systems can be done by illumination of a small water droplet (0.5–2 mm) with a He–Ne laser. For better observation, the laser should shine through an observation screen with a small aperture. If the laser beam diameter is larger than the drop size, Airy ring systems can readily be observed centered on the optical axis. It is advisable to use distilled water. Fresh tap water results in disturbances in the form of additional nonspherical fringes slowly crossing the interference pattern because of scattering at impurities etc. The patterns of distilled water are much more stable.

Part of the Airy ring systems of the primary bow are shown in Fig. 8 for two colinear red and green He–Ne lasers leading to the most simple system of supernumerary arcs, due to just two colors. It is easily possible to count more than 60 or 70 rings.

Because the ring systems of higher order may overlap with those of lower orders, it is convenient to use a He–Ne laser with a smaller diameter, which illuminates only one half of the drop. In this case, primary and secondary rainbows are at opposite sides such that more faint higher-order bows, lying in similar angular regions, are not obscured. Figure 9 is a photograph of four Airy ring patterns observed simultaneously on a wall. Clearly the brightest system belongs to the primary bow. From an analysis of the positions (see also Fig. 7), one readily deduces that the first-, second-, fifth-, and sixth-order ring systems are simultaneously seen. The third and the fourth orders are in the forward direction at ~45°. They, as well as other ring systems, can be seen when a screen is rotated around the water drop.

The observed Airy ring systems are not totally symmetric around the optical axis, as the water drop at the needle of the syringe is not perfectly spherical. Large drops are elongated because of gravitation, and near the needle, shape differences due to adhesion forces to the needle occur. They can lead to complex caustic effects, and quite spectacular displays can be observed. For quantitative measurements, one

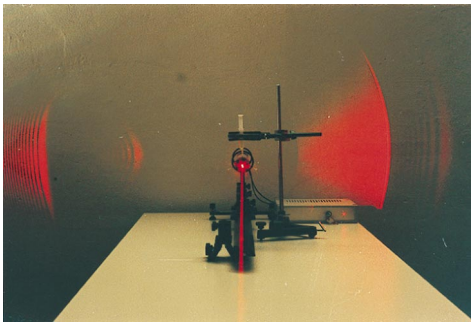

Fig. 9. Airy ring systems of first-, second-, fifth-, and sixth-order rainbows for a red He–Ne laser.

therefore usually refers to the horizontal plane where the cross section of the drop is spherical.

E. Quantitative Measurement of Airy Rings with Monochromatic Light Sources

The first quantitative measurements of Airy rings were published in the 19th century (see Ref. 16) in order to set the controversy among different theories of the rainbow. The results of these experiments finally helped the Airy wave theory of the rainbow to become generally accepted, although the more general Mie theory has produced measurable differences with Airy's theory (e.g., Refs. 13 and 14), which have meanwhile also been observed experimentally.

Quantitative experiments, i.e., measurements of the interference ring systems of the rainbow, can be done in at least two quite different ways, namely, first by studying spherical drops or second by studying cylinders.

1. Single Drops

In the first approach, spherical raindrops are illuminated by light. The easiest observation of the ring systems is, as described above, by shining with a laser onto a single water drop of e.g., 0.5-mm diameter. The angular dependence is measured with a precision rotary stage, and the scattered light intensity is monitored in a given direction.

In our experimental setup, we used a rotary stage of angular precision of 1/100° and monitored typically in intervals of 1/10° to 1/20°. Unfortunately, the measurement of an angular range from 110° to 150° takes several minutes. During this time, the drop evaporates i.e., decreases its size. Figure 10(a) demonstrates this problem. Even though the experiment was performed at a room temperature of ~15 °C, the drop suffered from a substantial evaporation. This results on the one hand in a change of the angular position of the Airy rings; on the other hand, the intensity of each ring depends on the size as well (e.g., Ref. 23). A water drop of initially ~2 mm evaporated during a time scale of ~15 min, quite appreciably leading to significant changes of the Airy ring intensities.

Every quantitative measurement of Airy rings has therefore to be analyzed carefully. An example of a

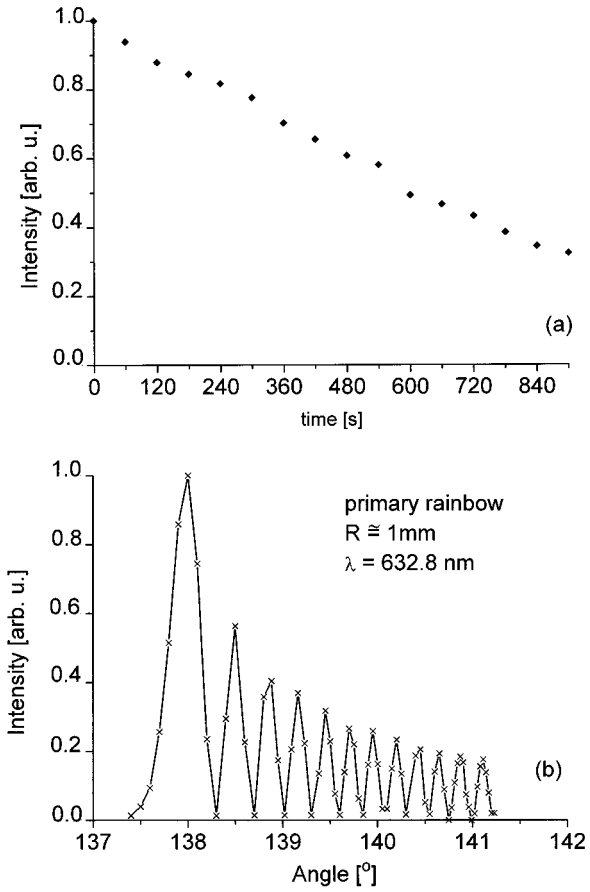

Fig. 10. Change of measured intensity of the first Airy ring maximum of the primary bow as a function of time. (a) The intensity decreases because of the decrease of the drop size, (b) Airy ring systems for a primary bow for a spherical water drop of $R \approx 1$ mm and $\lambda = 632.8$ nm. The intensities as functions of time were corrected according to (a).

quantitative measurement for a drop size of ~1 mm is shown in Fig. 10(b). Evaporation was accounted for by Fig. 10(a), i.e., the data at specific times were corrected such that the data should, to first order, represent Airy ring systems of the initial drop size (the change of angular positions with drop size was neglected).

2. Flowing Water

In order to improve the single-drop measurement we decided to use in a second approach cylindrical symmetry rather than a spherical one. This was already done by the first investigators, who used running water or thin glass cylinders (see Ref. 16). Illuminating perpendicularly leads to portions of the Airy ring systems in the plane perpendicular to the water flow.

In practice, a water container with a small hole (diameters between 0.4 and ≈2 mm) was used. In order to have steady flow, the hydrostatic pressure should be kept approximately constant within the water container. We used a very big water container, such that the water level is little affected by

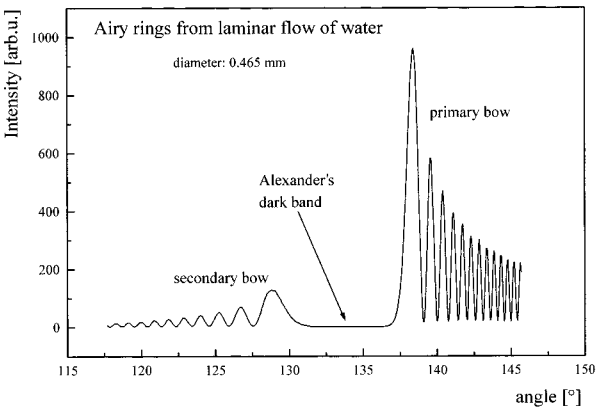

Fig. 11. Airy rings ($\lambda = 632.8$ nm) of primary and secondary bows for a cylinder of flowing water ($2R = 0.465$ mm).

the outflow through the thin nozzle. The maximum change of hydrostatic pressure was ~1%–2% during the measurement, which resulted in a change of intensity of the first Airy ring maximum of less than 2% over the time scale of the experiment. In this case, a change of rainbow angles could not be detected within the chosen step width of 0.05°. The size of the water cylinder was measured separately with a microscope. Figure 11 shows the result of a measurement of Airy rings for a water diameter of 0.465 mm.

The precision of the rotary stage was 0.01°, the angular resolution was 0.025°, the beam divergence was 0.42°, and data were taken in intervals of 0.05°. Clearly the differences in the primary and secondary ring systems can be seen. The first maximum is found at $\delta_{pri} = 138.4°$ for the primary bow and $\delta_{sec} \approx 128.8°$ for the broad maximum of the secondary bow.

In comparison, the Descartes theory would expect the maxima (for $n = 1.332$) at 137.8° and 129.4°, respectively. Mie theory for spherical symmetry would give rise to the primary maxima at 138.3° for $n = 1.332$ (courtesy E. Tränkle). It would be desirable to do a direct comparison with the theory for cylindrical symmetry also concerning the widths of the peaks. So far, it is already obvious, however, that such a simple setup can directly prove the validity of the wave theory of the rainbow.

Last but not least, it should be mentioned that the most spectacular experiments of rainbows concern realistic demonstrations with many water drops. Similar to rainbows in waterfall sprays, artificial rainbows can be observed in every garden or yard when water is sprinkled from a hose. By applying color filters one can, e.g., photographically detect infrared rainbows, demonstrating that the minimum-deviation effect is not restricted to the visual spectral range.[2] Supernumerary arcs can also be observed; however, drop size distributions and overlapping of all colors usually reduce the visibility to two or three Airy ring systems.

4. Halo Experiments

Halos in nature and their theoretical interpretation are discussed in many excellent articles and books (e.g., Refs. 2–4 and 24). In brief, halos are formed because of reflection and refraction effects in small hexagonal ice crystals. Because hexagonal crystals have a much larger geometric variety of light paths compared with that of raindrops, the number of possible related optical phenomena is larger, and today more than 40 different halo arcs, etc., are classified. Some of these, e.g., the parhelia that are due to minimum deviation of light by the ice crystals at a refracting angle of 60°, can be easily reproduced in experiments. Such demonstrations may on the one hand help us to understand the phenomena qualitatively; on the other hand they can provide quantitative data that help us to have a better theoretical understanding of more complex halo displays. Below, experiments to study parhelia (sun dogs), the parhelic circle, and Parry arcs are described. Many more experiments are possible.

A. Setup of Halo Experiments

The principle of halos may be illustrated, similarly to rainbow experiments, by a single model ice crystal. Depending on the halo phenomenon under study, slightly differing setups are necessary. The essential setup consists of a light source (white light or laser), a model ice crystal, a device for letting the ice crystal rotate, and a light detector. The rotation of the model crystal is necessary, as ice crystals have lower symmetry than spheres. In the atmosphere, crystals of all orientations (i.e., angles of incidence of light on various crystal faces) are possible. For a single crystal, this is modeled by the rapid rotation of the crystal, e.g., by a motor.

In this type of experiment, the angles of incidence are varied sequentially. Most detectors, such as the eye, yield time-averaged signals that therefore resemble halo displays. However, in a time-resolved detection mode, e.g., single pictures of a video sequence, only stroboscopic snapshots are seen, which bear no resemblence to naturally observed halos.

For qualitative experiments, the eye is the detector; for quantitative ones, photodiodes may be used. In addition, a rotary stage may be used for angular-resolved measurements. In this general setup, the following parameters may be varied:

- orientation of the rotating ice crystal model: c axis of crystal vertical, horizontal, or statistically distributed;
- angle of incidence of light: variation of angle models the Sun elevation;
- geometry of ice-crystal model: hexagons and triangles were used, but other forms are possible;
- material of ice-crystal model, changing the index of refraction: here, triangles of glass ($n = 1.62$) and hexagons made of Plexiglas ($n = 1.48$) were used.

For halos due to minimum deviation for refracting angles γ, the influence of the index of refraction n may be calculated from

$$\gamma_{\min} = 2 \arcsin\left(n \sin \frac{\gamma}{2}\right) - \gamma. \tag{3}$$

B. Experiments with a Glass Prism and White Light: Parhelia and Parhelic Circle

Parhelia are due to minimum deviation of the 60° angle of a hexagon. Therefore the basic effect can be demonstrated with a 60° prism. While illuminating the prism fully, one may slowly rotate the mount by hand to attribute the various light spots to reflection or refraction from various crystal faces. In the first experiment, the c axis should be perpendicular to the **k** vector of the incident light (i.e., Sun elevation = 0°). In particular, the light rays that are refracted twice give rise to the parhelia ray class. Because of dispersion of the prism the exiting spot resembles a nicely colored spectrum. While the angle of incidence is changed by rotation of the prism, the spectrum moves along the minimum-deviation curve (this is similar to the water drop rainbow experiment, in which the minimum-deviation curve for rainbow rays could also be traced directly). The minimum occurs for symmetric ray paths through the prism. This effect, well known by students from beginner labs, is usually used to determine the index of refraction of materials and to study the spectral lines of spectral lamps etc. However, the relation to atmospheric optics and parhelia is usually not mentioned.

After the effect is established by slow rotation, it is clear that rapid rotation of the crystal results in two halos, the spectrally resolved parhelia at the angle of minimum deviation due to twice-refracted rays and the parhelic circle due to single reflection. This situation is shown for a glass prism of $n = 1.62$ in Fig. 12. This experiment may be easily performed, with an overhead projector as the light source, by use of papers, books, etc., to form a slit that just illuminates the rotating prism. Compared with hexagonal ice crystals, our glass prism exhibits at least three differences, neglecting for the moment the geometric difference.

First, the higher index of refraction of $n = 1.62$ (ice has $n \approx 1.31$) changes the relative contributions of parhelia and the parhelic circle because of Fresnel equations. In particular, the parhelic circle is stronger than it would be for ice [for getting closer to ice, a hollow prism filled with water ($n \approx 1.33$) can be used; alternatively, the new development with easily machined and polished crystals of NaF with $n \approx 1.33$ at $\lambda = 640$ nm (Ref. 25) seems promising for the future]. This higher index of refraction also shifts the angular position of the parhelia [see Eq. (3)]. Second, ice is birefringent whereas glass is optically isotropic. Therefore the observable shift between the two parhelia components that can be observed in nature by the rotation of polarizing sheets by 90° cannot be seen here (see also Ref. 26). Third, glass has a larger dispersion than ice. Therefore the artificial parhelia are better spectrally resolved than those observed in nature.

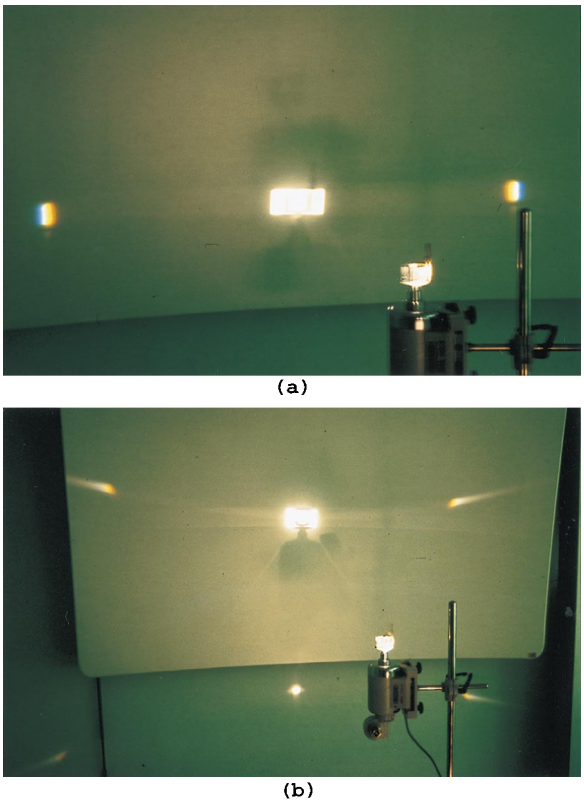

Fig. 12. Artificial parhelia and the parhelic circle as observed with a glass prism (n = 1.62) for a Sun elevation of (a) 0°, (b) ≈ 20°.

Changing the Sun elevation leads to a change of the halos, as shown in Fig. 12(b). These data are in qualitative agreement with Monte Carlo simulations.

C. Angular-Resolved Measurements of Parhelia and the Parhelic Circles

The experimental setup described in Subsection 4.B also allows angular-resolved measurements if the crystal rotates colinearly to the axis of a precision rotary stage on which a detector is mounted. With an expanded He–Ne laser as the monochromatic light source and an angular resolution of 0.15°, quantitative measurements of the intensity of parhelia and the parhelic circle at a Sun elevation of 0° were performed. These experiments were motivated by a discussion of the ray paths, which are responsible for certain features. In particular, some Monte Carlo simulations by Tränkle predicted features, known as 90° parhelia, that, compared with observations, were not uniquely accepted. The main points in the argument were the questions whether these features are indeed due to the predicted ray paths and, if so, whether they are observable in nature. The main problem of observations in nature is the contrast against the sky, as similarly bright changes of intensity could be due to changes in the concentration of ice crystals in a cloud, e.g., by contrails, etc.

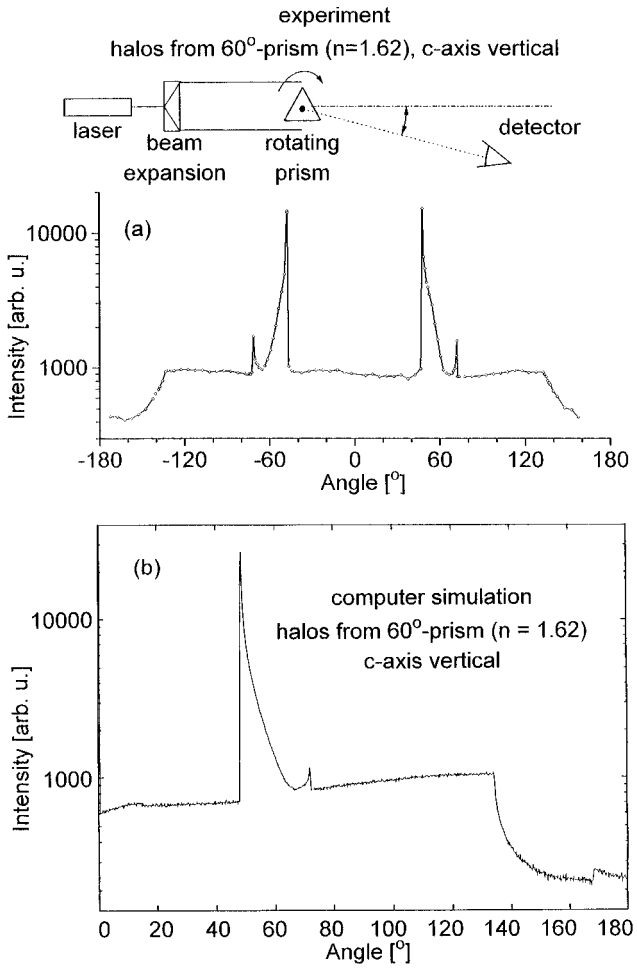

Fig. 13. (a) Intensities of parhelia and parhelic circles for a glass prism (n = 1.62) illuminated by a He–Ne laser (λ = 633 nm) as functions of the deviation angle, (b) Monte Carlo simulation of the experiment (courtesy E. Tränkle).

In order to solve this question experimentally, measurements at zero Sun elevation were performed with glass triangular prisms and Plexiglas hexagons. Measurements for higher Sun elevations are difficult, as, in this case, the signals are not on a circle at constant elevation. Therefore the detector would have to be adjusted in height while the angle was changed.

The results of the first quantitative measurement are shown in Fig. 13 for the glass prism (n = 1.62) together with a Monte Carlo simulation for this system by Tränkle.

Obviously the parhelia exhibit a strong peak, which rapidly decreases for increasing angle. At 72° an additional small peak can be seen not only by the photodiode, but also with the naked eye. It was this additional peak that motivated the whole experiment, as this structure, also seen in the simulation, corresponds to the so-called 90° parhelia for ice crystals.

After these preliminary studies, it was decided to approach more closely the natural phenomenon. Substituting the prism by a hexagon (n = 1.48) led to a much greater variety of ray paths, resulting in a more complex intensity pattern (see Fig. 14).

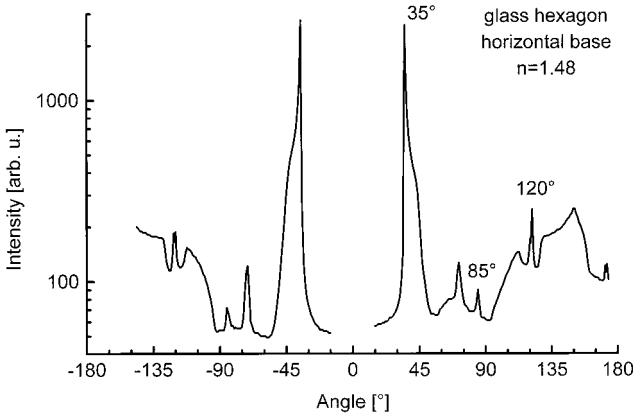

Fig. 14. Intensities of parhelia and parhelic circles for a glass hexagon (n = 1.48) illuminated by a He–Ne laser (λ = 633 nm) as functions of the deviation angle.

The various peaks can readily be attributed to certain ray classes. The experimental procedure is the following: The unexpanded laser (diameter ≈1 mm) is hitting the rotating hexagon (dimension ≈3 cm) and the horizontal position of the laser is shifted, until the desired feature is observed on a screen. Then the motor is stopped and the crystal is rotated slowly by hand. The various light spots that contribute to the desired feature can then be followed backwards, making an unequivocal interpretation possible. In a darkened room, the residual scattering of light within the hexagon may also allow direct visualization; however, it is more easy to observe the reflections simply at the side faces and follow their ray paths inside and outside the crystal. All features are also easily attributed to specific ray classes by use of Monte Carlo computer simulations. Obviously the 90° parhelia peak is located at ≈85°. Figure 15 shows the predicted ray path, giving rise to the 90° parhelia for zero Sun elevation.

Comparison between simulation and experiment clearly proves the existence of a feature at this angle. Therefore we conclude that the predicted halo feature must be present. After the existence of the predicted structures is unequivocally proved in the experiment, the open question obviously is whether they can be observed in nature, i.e., whether the intensity-to-background ratio is sufficient for natural observations (in the darkened laboratory, the 90° parhelia were visible to the naked eye also for the hexagon). Complications may arise, as the relative intensities of ray classes that contribute to certain features change as functions of Sun elevation. This holds for, e.g., the 120° parhelia but also for the 90° parhelia. As a matter of fact, the angular position of the 90° parhelia for ice crystals ranges from ≈98° (zero Sun elevation) to ~85° (Sun elevation 20°). At any rate we still have to wait for the first unequivocally verified observation of 90° parhelia. Maybe they will be found for a Sun elevation close to zero, where they should be observable with the naked eye.

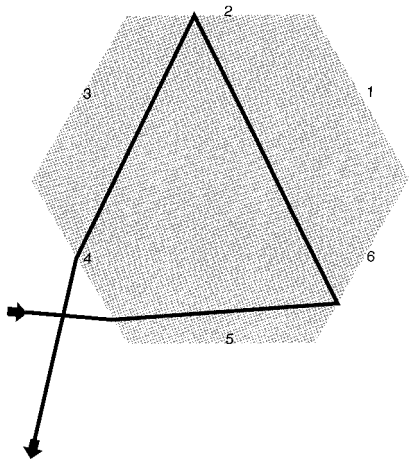

Fig. 15. Theoretical ray path responsible for the 90° parhelia.

D. Historical Chemical Recipes for Ring Halos

There are a large number of historical chemical recipes for producing ring halos. The basic idea is the generation of crystals by precipitation from a saturated solution (e.g., Refs. 20 and 27). In particular Cornu used an idea of Brewster, who observed the Sun through a glass plate, covered with dried alaun ($KAl(SO_4)_7 \cdot 12\ H_2O$) crystals. Three rings of $\approx$18.3°, 29.5°, and 40°–45° could be observed in the transmitted light, which can be attributed to minimum-deviation effects from the cubic crystals with pyramids on end faces with octahedral and dodecahedral symmetry.

Cornu developed another recipe that works without drying the crystals. A cold saturated solution of alaun ($n \approx 1.3$) is illuminated with white light or a laser. Adding ~10%–15% alcohol (at least 90%) and shaking the mixture soon leads to the generation of alaun crystals that attenuate the transmitted light. In a dark room, one may soon observe ring halos. According to Pernter[20] two rings (9.5° and 20°) may be visible. The observation time depends on the number and the size of crystals as well as on the quality of their surfaces. Hence one just has to try the best empirical recipe (good luck and persistence).

E. Other Halos

In addition to parhelia, ring halos, and the parhelic circle, there are many other halo phenomena that can be observed experimentally. Two of the most brilliant arcs, the circumzenithal and the circumhorizontal arcs (due to crystals with c axes vertical and a refracting angle of 90°), are, unfortunately, observable only for crystals with an index of refraction of $n < \sqrt{2}$. Hence they are not observable with the glass prisms and hexagons. It is, however, possible, to observe these arcs by use of a hollow hexagon (made of microscope slides) filled with water.[28]

Parry arcs, alternate Parry arcs, and tangent arcs may be easily demonstrated for various Sun elevations by illumination of the rotating hexagon columns with the appropriate orientation. Figure 16 shows

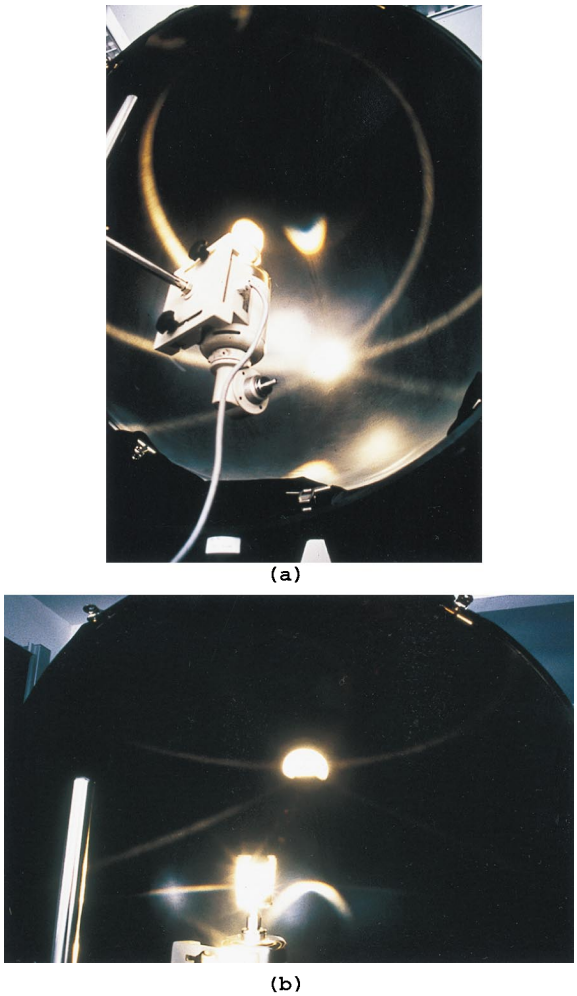

Fig. 16. Halo display due to hexagons (n = 1.48), rotating in Parry arc orientation and illuminated with white light from a slide projector. Sun elevations of (a) 0°, (b) ≈40° were chosen. The halos were projected on a hemisphere of 1-m diameter.

two examples. The crystals were in Parry arc orientation and Sun elevations were 0° and 40°. In order to observe large portions of the halo, the crystals were rotated in the center of a hemisphere of ~1-m diameter, whose inner side served as a hemispherical projection screen.

In addition to generating the arcs, all polarization effects of halos may be tested experimentally by polarizing sheets. Parallel light and perpendicular polarized light give rise to different intensities, as described by Fresnel equations (see Ref. 26).

5. Conclusions

A survey of laboratory experiments on atmospheric optics, in particular mirages, rainbows, and halos, is presented. Besides serving didactical purposes (providing easy and impressive qualitative lecture demonstrations at various levels of difficulty, e.g., direct visualization of the minimum-deviation curve for rainbow paths in water droplets), quantitative experiments allow direct comparison of angular positions and intensities with analytical computations or Monte

Carlo simulations of these light-scattering phenomena. Hence laboratory experiments on atmospheric optics are useful complements to visual observations as well as photographs on the one hand and theoretical models and explanations on the other.

We thank B. Görtz, J. Schmidt, and D. Karstädt for help with some experiments, Ken Sassen for sending a NaF crystal, and in particular E. Tränkle for motivating the halo experiments and providing theoretical plots.

References

1. M. G. J. Minnaert, *Light and Color in the Outdoors* (Springer, Berlin, 1993); English edition entitled *The Nature of Light and Colour in the Open Air* (Dover, New York, 1954).
2. R. Greenler, *Rainbows, Halos and Glories* (Cambridge U. Press, Cambridge, 1980).
3. W. Tape, *Atmospheric Halos* (American Geophysical Society, Washington, D.C., 1994).
4. D. K. Lynch and W. Livingston, *Color and Light in Nature* (Cambridge U. Press, Cambridge, 1995).
5. Feature issue on light and color, J. Opt. Soc. Am. A **4,** (1987); Appl. Opt. **30,**(24) (1991); Appl. Opt. **33,**(21) (1994).
6. J. Müller, *Atlas zum Lehrbuch der Kosmischen Physik* (Vieweg, Braunschweig, 1856).
7. R. Greenler, "Laboratory simulation of inferior and superior mirages," J. Opt. Soc. Am. A **4,** 589–590 (1987).
8. R. W. Pohl, *Einführung in die Physik: Optik und Atomphysik*, 9th ed. (Springer, Berlin, 1954).
9. W. A. Strouse, "Bouncing light beam," Am. J. Phys. **40,** 913–914 (1972).
10. R. W. Wood, "Some experiments on artificial mirages and tornadoes," Philos. Mag. **47,** 349–353 (1899).
11. *Fata Morganen—Zauberspiegel am Horizont*, television film produced by M. Engler, First Broadcast 8 March 1996 by ARTE.
12. C. Tape, "Mirages," presented at the conference on Light and Color in the Open Air, Santa Fe, New Mexico, February 1997.
13. H. C. van de Hulst, *Light Scattering by Small Particles* (Dover, New York, 1981).
14. C. F. Bohren and D. R. Huffman, *Absorption and Scattering of Light by Small Particles* (Wiley, New York, 1983).
15. U. Kreibig and M. Vollmer, *Optical Properties of Metal Clusters*, Vol. 25 of the Springer Series on Material Sciences (Springer-Verlag, New York, 1995).
16. C. F. Boyer, *The Rainbow: From Myth to Mathematics* (Princeton U. Press, Princeton, N.J., 1987).
17. Oeuvres de Descartes, Charles Adam and Paul Tannery, eds., Discours de la Méthode et Essais VI: Les Meteors–Discours VIII de l'Arc en Ciel (1637) (Vrin, Paris, 1982).
18. I. Newton, *Opticks: or a Treatise of the Reflexions, Refractions, Inflexions and Colours* (Royal Society, London, 1704); (German ed. Vieweg, Braunschweig, 1983).
19. H. M. Nussenzveig, "The theory of the rainbow," Sci. Am. **237,** 116–127 (1977); "Complex angular momentum theory of the rainbow and the glory," J. Opt. Soc. Am. **69,** 1068–1079 (1979).
20. J. M. Pernter and F. M. Exner, *Meteorologische Optik*, 2nd ed. (Braumüller, Vienna, 1922).
21. J. Walker, "Multiple rainbows from single drops of water and other liquids," Am. J. Phys. **44,** 421–433 (1976); "How to create and observe a dozen rainbows in a single drop of water," Sci. Am. **237,** 138–144 (1977); "Mysteries of rainbows, notably their rare supernumerary arcs," Sci. Am. **240,** 146–152 (1980).
22. K. Sassen, "Angular scattering and rainbow formation in pendant drops," J. Opt. Soc. Am. **69,** 1083–1089 (1979).
23. A. B. Fraser, "Why can the supernumerary bows be seen in a rain shower?," J. Opt. Soc. Am. **73,** 1626–1628 (1983).
24. E. Tränkle and R. G. Greenler, "Multiple-scattering effects in halo phenomena," J. Opt. Soc. Am. A **4,** 591–599 (1987).
25. K. Sassen, Department of Meteorology, University of Utah, Salt Lake City, Utah 84112 (personal communication, February 1997).
26. G. P. Können and J. Tinbergen, *Polarized Light in Nature* (Cambridge U. Press, Cambridge, 1985); "Polarization structures in parhelic circles and in 120° parhelia," Appl. Opt. **37,** 1457–1464 (1998).
27. L. Bergmann and C. Schäfer, *Lehrbuch der Experimentalphysik III: Optik*, 7th ed. (de Gruyter, Berlin, 1978).
28. R. Greenler, Department of Physics, University of Wisconsin-Milwaukee, Milwaukee, Wis. 53201 (personal communication, February 1997).